PERFORMANCES OF L-SHAPE SHEAR CONNECTOR SUBJECTEDTO STRUT COMPRESSIVE FORCE IN STEEL-CONCRETE COMPOSITE STRUCTURES

R. SOTY[1*] and H. SHIMA[2]

[1]*Depatment of infrastructure Systems Engineering, Kochi University of Technology, Japan*
[2]*Depatment of infrastructure Systems Engineering, Kochi University of Technology, Japan*

ABSTRACT

This paper presents the performances of L-shape shear connector subjected to strut compressive force in steel-concrete composite structures. L-shape shear connectors were found to fail in two different failure modes, split failure mode, and concrete crushed/shear failure mode depending of the direction of the strut compressive force. There existed a critical strut angle separating the two different failure modes, and it was found to have a linear relationship with the thickness to height ratio of the shear connector. Meanwhile, a design equation for the ultimate shear capacity of the shear connector for each failure mode was developed and proposed. It was confirmed that the shear force-relative displacement relationship could be represented by a unique enveloped curve by normalizing the shear forces by the ultimate shear force and the relative displacements by the height of the shear connector. Thus, an exponential equation to predict the enveloped curve was proposed while the ultimate relative displacement was found approximately 0.02 times the height of the shear connectors regardless of the sizes of the shear connector, the concrete strength, and the strut angle.

Keywords: L-shape shear connector, strut compressive force, shear force, relative displacement.

1. INTRODUCTION

L-shape shear connector is one of shear connector type which is usually used to transfer shear force from steel to concrete and vice versa in steel-concrete composite structures. The equation to predict the shear capacity of L-shape shear connector was previously given by (JSCE 1992 and 2006). However, according (Soty and Shima 2010 and 2011), the equations given by (JSCE 1992 and 2006) were found to underestimate the shear capacity of L-shape shear connector subjected to strut compressive force. Then a new equation was subsequently developed and proposed. They (Soty and Shima 2010) proposed not only the equation to predict the shear capacity but also that to predict the shear force-relative displacement relationship of L-shape shear connector based on the experimental results of 1st series specimens and the FEM analyses results. However, their equations were proposed only in cased of strut angle of 45° and splitting crack controlled the final failure mode.

Therefore, this paper integrates the experimental results of (Soty and Shima 2010) with the test results of a 2nd series specimens whose strut angles are smaller than 45° ($\theta < 45^o$) in order to

* Corresponding author: Email: ros.soty@kochi-tech.ac.jp

propose new equations for the ultimate shear forces of L-shape shear connector V_u at split failure and at shear failure. This paper also proves the applicable ranges of the formula of the enveloped curve of shear force-relative displacement relationship of the shear connectors which was previously proposed by (Soty and Shima 2010) in case of different failure modes and strut angles.

2. EXPERIMENT

The specimens are symbolized as S-height of specimen-height of shear connector-thickness of shear connector-concrete strength-strut angle (S-h-h_{sc}-$t_{1,sc}$-f_c'-θ). Figure 1 and Table 1 give the detail of both the 1st and the 2nd test series specimens including the shear connector and the support. JIS G 3101 standard steel with grade SM490 (f_y=370N/mm^2, f_u=511N/mm^2 and E=204kN/mm^2) and grade SS400 (f_y=352N/mm^2, f_u=448N/mm^2 and E=202kN/mm^2) was used for the steel skin plate and the shear connector, respectively. The mix proportions of concrete used for all specimens are summarized in Table 2.

Strain distributions in the skin plate in front of the shear connector were measured by strain gauges of 5 mm long, R1-R2 and R3-R4 attached on both sides of the skin plate as shown in Figure 2a. However, differently from the 1st test series specimens, strain gauges R5-R6 were also mounted on both sides of the shear connectors in the 2nd test series specimens. The distribution of concrete-skin plate slip in front of the shear connector was measured by means of the displacement transducers as illustrated in Figure 2b. The average value given by LD1-LD4 was determined as the slip. Figure 2c illustrates how the relative displacements between the top and the bottom of the shear connector δ

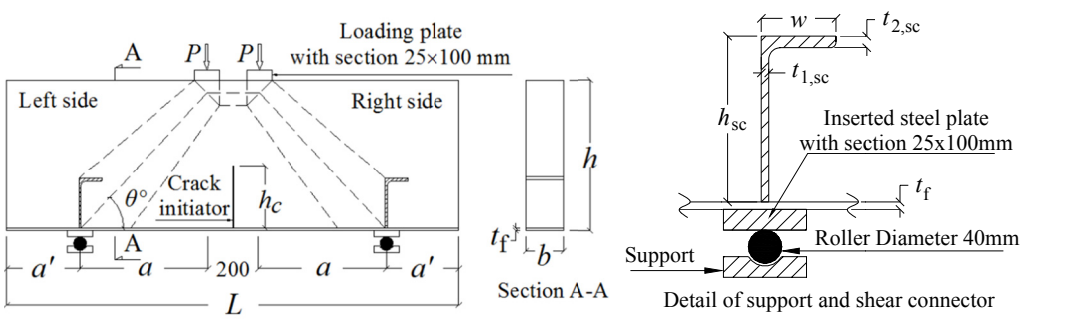

a) Detail of beam type specimens b) Detail of shear connector and support

Figure 1: Detail of specimens and support.

Table 1: Detail of all specimens

Specimens	Sizes of Specimens (mm)							Shear connectors (mm)				Skin plate	f_c'
	a	b	h	L	a'	θ(°)	h_c	h_{sc}	w	$t_{1,sc}$	$t_{2,sc}$	t_f (mm)	(N/mm^2)
S-600-200-9-38-45	510	150	600	1800	300	45	-	200	90	9	14	9	38.0
S-600-200-9-25.3-45	510	150	600	1800	300	45	-	200	90	9	14	9	25.3
S-450-150-9-23.6-45	410	150	450	1500	250	45	-	150	75	9	14	9	23.6
S-300-100-9-25.1-45	290	150	300	1100	200	45	-	100	50	9	14	9	25.1
S-600-200-9-43-30	950	150	600	2700	300	30	300	200	90	9	14	9	43.0
S-600-200-9-43-35	750	150	600	2300	300	35	300	200	90	9	14	9	43.0
S-450-150-9-43-25	850	150	450	2400	250	25	250	150	75	9	14	9	43.0
S-450-150-9-43-30	650	150	450	2000	250	30	250	150	75	9	14	9	43.0
S-300-100-9-42.7-20	650	150	300	1900	200	20	150	100	50	9	14	9	42.7
S-300-100-9-41.5-25	500	150	300	1600	200	25	150	100	50	9	14	9	41.5

Table 2: Mix proportions of concrete product

Specimens	Slump (cm)	W/C (%)	s/a (%)	Unit weight (kg/m^3) Water	Cement	Sand	Aggregate	WRA*	AEA**
S-600-200-9-38-45	18	46	40	175	378	695	1059	3.78	15.1
S-600-200-9-25.3-45									
S-450-150-9-23.6-45	8	73	45	155	211	876	1070	2.11	8.4
S-300-100-9-25.1-45									
2nd Test Series	18	54	48.8	175	342	520	921	2.5	1.62

* Water Reducing Admixture, ** Air Entraining Agent

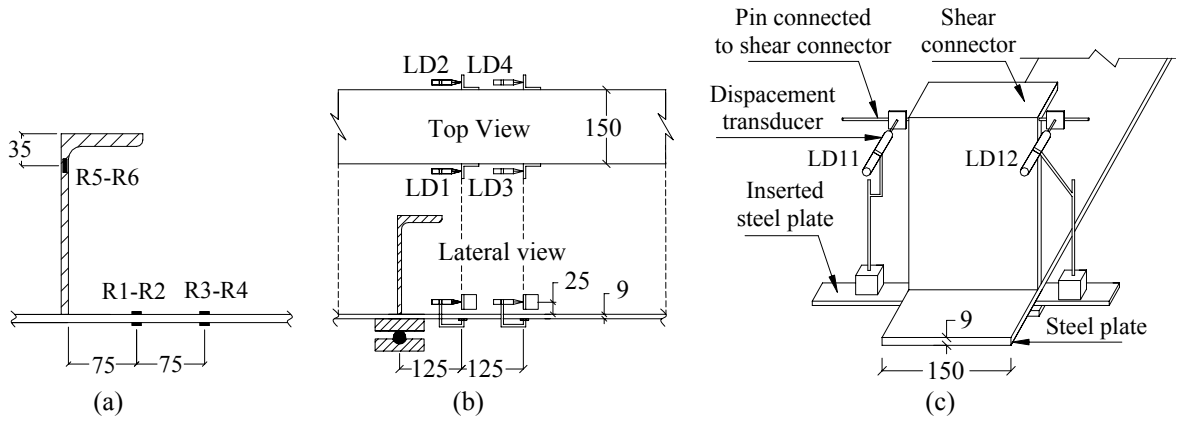

Figure 2: (a) Locations of strain gauges; (b) Slip measurement location; (c) Locations of displacement transducers for relative displacement measurement.

were measured. The strain gauges and the displacement transducers were installed left-right symmetrically in pairs in all specimens. The specimens were loaded and unloaded with an increment of 30kN; meanwhile, the load *P* and the data from the strain gauges and the displacement transducers were recorded until failure of the shear connector.

3. PERFORMANCE OF L-SHAPE SHEAR CONNECTOR

3.1. Failure Mode

L-shape shear connectors were found to fail with different failure modes, split failure, shear-split failure, concrete crush, and shear failure were identified. The conditions of the shear connectors at failures observed in the 2nd test series specimens are illustrated in Figure 3. The experimental results showed that the possibility of split failure and concrete crush or shear failure depended on the strut angle θ and the size of the shear connector. Accordingly, the relationships between θ and $t_{1,sc}/h_{sc}$ of all tested specimens were plotted in Figure 4. The experimental results suggested that split failure mode and concrete crush or shear failure mode of the shear connector can be separated by a border line of a critical strut angle θ_o which is a function of $t_{1,sc}/h_{sc}$ as expressed in equation (1).

$$\theta_o = -210 \times \left(t_{1,sc} / h_{sc}\right) + 41 \tag{1}$$

Where, θ_o: critical strut angle (deg), $t_{1,sc}$: thickness of the shear connector, and h_{sc}: height of the shear connector.

It means that split failure mode and concrete crush or shear failure mode would occurred when strut angle $\theta > \theta_o$ and $\theta \leq \theta_o$, respectively.

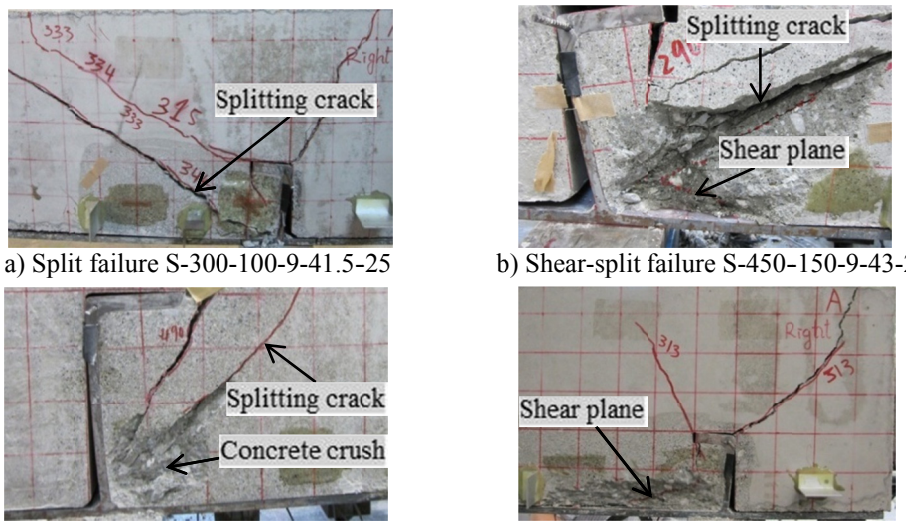

a) Split failure S-300-100-9-41.5-25 b) Shear-split failure S-450-150-9-43-25

c) Concrete crush-split failure S-600-200-9-43-35 d) Shear failure S-300-100-9-42.7-20

Figure 3: Different failure modes of shear connectors in 2nd test series specimens.

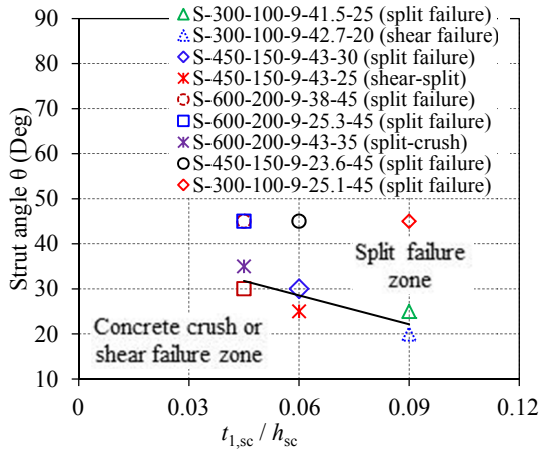

Figure 4: Relationship between θ and $t_{1,sc}/h_{sc}$.

The different performance of L-shape shear connectors subjected to strut compressive force F failed in split failure mode and in concrete crush or shear failure mode can be simply explained by Figures 5a and 5b and Figures 5c and 5d, respectively. As shown in Figure 5a, when $\theta > \theta_o$ the concrete in front of the shear connector seemed to resist against multi-direction stresses; and the release of the principal tensile stress σ_t depended on the relative displacement δ. Then, when the relative displacement reached its ultimate value δ_u, splitting crack took place in the concrete along the compressive strut axis perpendicular to the principal tensile stress direction, Figure 5b.

Differently, as shown in Figure 5c, when $\theta \leq \theta_o$ the concrete in front of the shear connector was forced to relocate from the crushing point and moved along the direction of the principal tensile stress σ_t. This mechanism induced a vertical confinement of concrete in front of the shear connector and resulted in high tensile stress in the vertical part of the shear connector. Due to the vertical confinement upon the concrete, due to the relative displacement of the shear connector, and due to the strut compressive force with $\theta \leq \theta_o$, the concrete in front of the shear connector failed in concrete crush or shear failure mode at ultimate relative displacement δ_u and at a shear compressive

stress τ forming a shear plane as shown in Figures 3d and 5d.

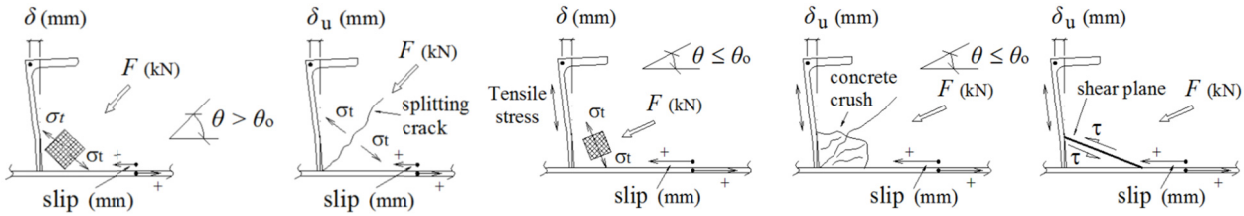

a) Before split failure b) At split failure c) Before shear failure d) At concrete crush or shear failure

Figure 5: L-shape shear connector with ($\theta > \theta_o$) and with ($\theta \leq \theta_o$).

3.2. Ultimate shear force

Table 3 gives a summary of the ultimate shear forces $V_{u.exp}$ obtained from experimental results and calculation results V_{sc1} by means the formula given by (JSCE 2006) with all safety factors 1.0. It can be observed that $V_{u.exp}/V_{sc1}$ was found up to 1.69 when θ was small. This meant that JSCE's equation gave a conservative prediction. Similarly, the shear force $V_{u.sc2}$ predicted by means of the equation given by (Soty and Shima 2010) was also found conservative when $\theta < 45^o$ with $V_{u.exp}/V_{u.sc2}$=1.25. Therefore, new formulas for the ultimate shear forces of L-shape shear connectors V_u failed in split failure mode and in concrete crush or shear failure mode are necessary. Based on a simplified model given in Figure 6, the formulas to predict the shear capacity of the shear connector were developed and proposed as follows:

$$V_u = k \times (f_c')^{0.5} \times b_{sc} \times h_{sc} \times \cos\theta \quad (2)$$

$$k = 28 \times (t_{1,sc}/h_{sc}) + 0.7 \quad \text{if} \quad \theta \succ \theta_o \quad (3)$$

$$k = 36 \times (t_{1,sc}/h_{sc}) + 0.66 \quad \text{if} \quad \theta \leq \theta_o \quad (4)$$

Where, V_u: ultimate shear force in concrete crush or shear failure mode (N), b_{sc}: width of shear connector (mm), h_{sc}: height of shear connector (mm), $t_{1,sc}$: thickness of shear connector (mm), f_c': concrete compressive strength (N/mm^2), and θ: strut angle ($\theta \leq \theta_o$) (degree).

It can be seen in Table 3 that equation (2) can precisely predict the ultimate shear force with $V_{u.exp}/V_{u.Eq2}$ varied from 1.00 to 1.04.

Table 3: Ultimate shear force obtained from experiment and calculation results

Specimens	$V_{u.exp}$ (kN)	V_{sc1} (kN)	$V_{u.exp}/V_{sc1}$	$V_{u.sc2}$ (kN)	$V_{u.exp}/V_{u.sc2}$	$V_{u.Eq.2}$ (kN)	$V_{u.exp}/V_{u.Eq2}$
S-600-200-9-38-45	266	240	1.11	254	1.05	254	1.05
S-600-200-9-25.3-45	200	195	1.02	207	0.96	207	0.96
S-450-150-9-23.6-45	180	171	1.06	182	0.98	182	0.98
S-300-100-9-25.1-45	170	154	1.11	169	1.00	169	1.00
S-300-100-9-41.5-25	272	198	1.37	218	1.25	282	0.97
S-600-200-9-43-35	362	254	1.42	-	-	-	-
S-600-200-9-43-30	388	254	1.53	-	-	388	1.00
S-450-150-9-43-30	357	231	1.54	-	-	-	-
S-450-150-9-43-25	391	231	1.69	-	-	377	1.04
S-300-100-9-42.7-20	360	202	1.63	-	-	359	1.00

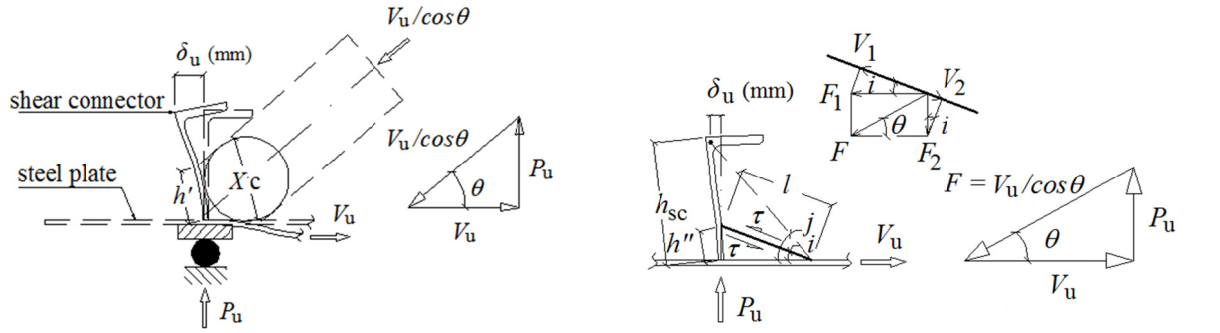

a) Model of shear connector in split failure mode

b) Model of shear connector failed in shear failure mode

Figure 6: Model of L-shape shear connector at failure.

3.3. Shear force-slip relationship

As shown in Figure 7, it was found that slip between concrete and skin plate in front of the shear connector appeared even under low load levels. Similar results were also found by (Kiyomiya et al. 1986), (Ueda and Chin 1989), and (Chuah et al. 1991). However, L-shape shear connectors in beam type specimens were found to have shear resistance even though the diagonal crack already appeared in the concrete from the head of the shear connector. These results proved the advantage of the test method as compared to push-out and pull-out test methods. Based on the experimental results of (Kiyomiya et al. 1986), (Ueda and Chin 1989), and (Chuah et al. 1991), the shear connectors in push-out and pull-out tests gradually lose their shear resisting abilities after crack appeared in the concrete from the head of the shear connectors. Meanwhile, no effect of shear connector height on shear force-slip relationships was observed. However, based on the experimental results, the failure mode of the shear connector and the strut angle were found to have an effect on the ultimate shear force and the ultimate slip.

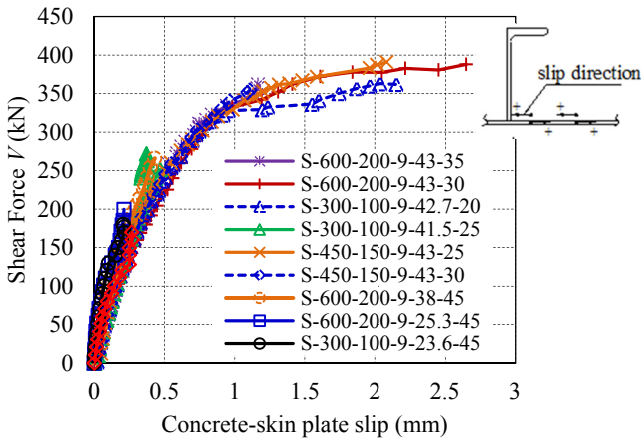

Figure 7: Shear force-slip relationships.

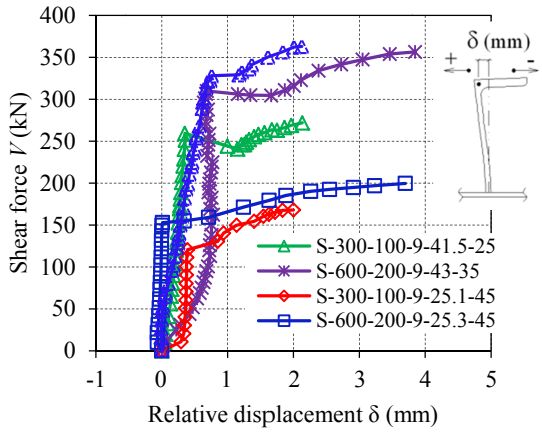

Figure 8: *V*-*δ* relationships.

3.4. Shear force-relative displacement relationship

It can be observed in Figure 8 that large increment of relative displacement with small increment of shear force appeared after the diagonal crack appeared from the head of the shear connector. These results indicated that the stiffness of the shear connector was suddenly reduced by the occurrence of

the first diagonal crack. These similar behaviors were also observed in steel-concrete sandwich beams by (Saidi et al. 1999 and 2008). More importantly, the experimental results suggested that the relative displacement of the shear connector has a great influence on its shear resisting capacity. The displacement of the head of the shear connector caused a release of the principal tensile stress generated in the concrete in front of the shear connector. This phenomenon limited the level of shear force on the shear connector. Therefore, the relative displacement of the shear connector has to be carefully controlled in design. Advantageously, the ultimate relative displacements δ_u, the displacement which caused failure of shear connector, and the ultimate shear forces V_u of L-shape shear connectors were obtained in this study.

3.5. Formulation for shear force-relative displacement relationship

The formula for shear force-relative displacement relationship of L-shape shear connector subjected to strut compressive force was previously given by (Soty and Shima 2010). It was proposed only in case of $\theta = 45^o$ and for the case after the occurrence of diagonal crack from the head of the shear connector until failure of the shear connector, where the shapes of the curves were experimentally clearly observed. The equation was given as follows:

$$V/V_u = \left(1 - \exp\left(-180 \times \left(\delta/h_{sc}\right)\right)\right)^{0.6} \tag{5}$$

Where, V_u: ultimate shear force of the shear connector (N), δ: relative displacement (mm), and h_{sc}: height of shear connector (mm).

Figure 9 gives V/V_u and δ/h_{sc} relationships of the 1st and the 2nd test series specimens with different strut angle and failure mode. It can be observed that good agreements between the experimental results and the calculation results by means of equation (5) were also observed regardless of the strut angle and the size of the shear connector. Therefore, these results implied that equation (5) could be used to predict the enveloped curve of shear force-relative displacement relationships of L-shape shear connector regardless of the size of the shear connector, the strut angle, the concrete strength, and the final failure mode. Meanwhile, δ_u was confirmed to be equal to $0.02h_{sc}$.

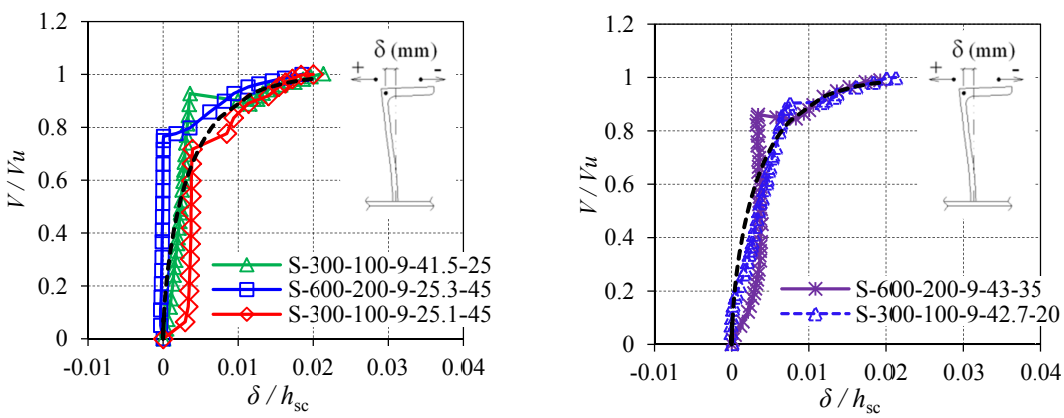

(a) Split failure specimens

(b) Concrete crush or shear failure specimens

Figure 9: V/V_u – δ/h_{sc} relationships.

4. CONCLUSIONS

(1) L-shape shear connectors under strut compressive forces in steel-concrete composite structures were found to have different failure modes namely split failure mode and concrete crush or shear failure mode. Both final failure mode and shear resisting mechanisms of the shear connector were found to be controlled by the strut angle and the thickness to height ratio of the shear connector.

(2) There existed a critical strut angle θ_o separating split failure mode from concrete crush or shear failure mode regardless of concrete strength. The equation of θ_o was found to be linear whose equation was a function of thickness to height ratio of the shear connector as given in equation (1).

(3) The equation to predict the ultimate shear capacity V_u of L-shape shear connector subjected to strut compressive force was developed and proposed as appeared in equation (2). However, the applicable ranges of the proposed equations are only in the interval of strut angle $20^o \leq \theta \leq 45^o$.

(4) Regardless of the size of the shear connector, the concrete strength, and the strut angle, the relationship between shear force and relative displacement of L-shape shear connector can be represented by a unique enveloped curve by normalizing the shear forces by the ultimate shear force and the relative displacements by the height of the shear connector for the case after the occurrence of diagonal crack from the head of the shear connector until failure of the shear connector. The ultimate relative displacements δ_u of L-shape shear connectors was found approximately 0.02 times the height of the shear connector.

(5) By means of this research results, the applicable ranges of equation (5) was extended to be applicable to predict the enveloped curved of shear force-relative displacement relationship of L-shape shear connector despite different shear connector sizes, concrete strength, and strut angle.

5. REFERENCES

Chuah CL, Shima H and Virach R (1991). Load-displacement relationship of plate shear connector in steel-concrete composite structure. Proc. of JSCE, 15(43), pp. 223-229.

JSCE Research Subcommittee on steel-concrete sandwich structures (1992). Design code for steel-concrete sandwich structures-draft-. Concrete Library International, JSCE, No.20.

JSCE Guidelines for performance verification of steel-concrete hybrid structures (2006). Hybrid Structure Series 2, Japan Society of Civil Engineers.

Kiyomiya O, Yokota H, Suzuki M and Chiba T (1986). Strength properties of shear connector by shape steel. Transaction of the Japan Concrete Institute, JCI, 8, pp. 345-352.

Saidi T, Furuuchi H and Ueda T (1999). Effect of shape and location of shear connector on its transferred shear force and relative displacement relationship in steel-concrete sandwich beam. Journal of Structural Engineering, JSCE, 45(A), pp. 1451-1459.

Saidi T, Furuuchi H and Ueda T (2008). The transferred shear force-relative displacement relationship of the shear connector in steel-concrete sandwich beam and its model. Doboku Gakkai Ronbunshuu, E, 64(1), pp. 122-141.

Soty R and Shima H (2010). Shear force-horizontal relative displacement relationship of L-shape shear connector subjected to strut compressive force in steel-concrete composite structures. Journal of Structural Eng./Earthquake Eng., JSCE, 27 (2), pp. 56s-71s. (Copy of Doboku Gakkai Ronbunshuu A 2010.12; 66 (4), pp. 767-782.

Soty R and Shima H (2011). Formulation for maximum shear force on L-shape shear connector subjected to strut compressive force at splitting crack occurrence in steel-concrete composite structures. Procedia Engineering, 14, pp. 2420-2428.

Ueda T and Chin CK (1989). Strength of steel plate shear connector. Proc. of Second Symposium on Research and Application of Composite Constructions, JSCE, pp. 149-156. (in Japanese)